PHYSICAL REVIEW B **76**, 184414 (2007)

# Nonresonant microwave absorption in epitaxial $La_{0.7}Sr_{0.3}MnO_3$ films and its relation to colossal magnetoresistance

M. Golosovsky* and P. Monod
*Laboratoire de Physique du Solide, ESPCI, 10 rue Vauquelin, 75231 Paris Cedex 05, France*

P. K. Muduli and R. C. Budhani
*Department of Physics, Indian Institute of Technology, Kanpur, 208016, India*

L. Mechin and P. Perna†
*GREYC (CNRS-UMR 6072), ENSICAEN and University of Caen, 6 Blvd Marechal Juin-14050, Caen-Cedex, France*
(Received 18 June 2007; published 13 November 2007)

We study magnetic-field-dependent nonresonant microwave absorption and dispersion in thin $La_{0.7}Sr_{0.3}MnO_3$ films and show that it originates from colossal magnetoresistance. We develop a model for the magnetoresistance of a thin ferromagnetic film in an oblique magnetic field. The model accounts fairly well for our experimental findings, as well as for the results of other researchers. We demonstrate that nonresonant microwave absorption is a powerful technique that allows contactless measurement of magnetic properties of thin films, including magnetoresistance, anisotropy field, and coercive field.

DOI: 10.1103/PhysRevB.76.184414 PACS number(s): 75.47.Lx, 75.47.Gk, 76.50.+g, 75.70.−i

## I. INTRODUCTION

The colossal magnetoresistance of manganites has been extensively studied by transport methods and was attributed to the double-exchange mechanism,[1] although the detailed mechanism has not been unambiguously established so far. This encourages experimental study of magnetoresistance in manganites by complementary methods. Contactless techniques, such as microwave absorption, are particularly advantageous here. This is the purpose of our present study: to explore potential of the microwave absorption technique to measure magnetoresistance in manganites.

So far, microwave absorption in manganites has been studied by the cavity perturbation technique. The measurements in constant field[2–4] revealed microwave absorption linearly dependent on magnetic field that was attributed to colossal magnetoresistance. The measurements in alternating field, using the field modulation technique,[5–7] revealed a very broad nonresonant absorption. Lyfar *et al.*[7] assumed that it originates from the colossal magnetoresistance (CMR) as well. In this work we systematically study the field and angular dependence of nonresonant microwave absorption in epitaxial $La_{0.7}Sr_{0.3}MnO_3$ films and prove its magnetoresistive origin.

We perform our measurements using a Bruker *X*-band electron-spin-resonance (ESR) spectrometer equipped with a bipolar current source. While such spectrometers are widely used for magnetic resonance measurements, their employment for the study of nonresonant microwave absorption has been restricted mostly to superconductors.[8] In this work we develop a methodology to analyze the nonresonant microwave absorption measured using the ESR spectrometer and field modulation techniques. Since the ESR technique is very sensitive and versatile, our approach opens a powerful opportunity to study the magnetoresistance of different materials in a contactless way.

## II. MODEL

### A. Ferromagnetic film in oblique magnetic field: Magnetostatics

To calculate magnetization of a thin ferromagnetic film in oblique magnetic field we consider its free energy

$$\Phi = \Phi_0(M) + U_{anisotropy} + U_{demagnetization} + U_{Zeeman}. \quad (1)$$

The first term here absorbs all angular-independent contributions. We approximate it by $\Phi_0(M)=\frac{(M-M_0)^2}{2\chi_0}+\text{const}$, where $M_0$ is the zero-field magnetization and $\chi_0=\frac{dM}{dH}$ is the bulk magnetic susceptibility. We assume the "easy-plane" anisotropy (this includes the shape and the crystalline anisotropy); hence, $U_{anisotropy}+U_{\text{demagnetization}}=\frac{\beta M^2}{2}\cos^2\Theta$, where $\Theta$ is the polar angle of magnetization, $\Psi$ is the polar angle of the external field, and $\beta>0$. The anisotropy field is $H_a=\beta M$. Equation (1) reads then

$$\Phi(M,\Theta) = \frac{(M-M_0)^2}{2\chi_0} + \frac{\beta M^2}{2}\cos^2\Theta - MH\cos(\Theta-\Psi), \quad (2)$$

where we retain only those terms that depend on $M$ and $\Theta$. The equilibrium conditions $\left(\frac{\delta\Phi}{\delta\Theta}\right)_M=0$; $\left(\frac{\delta\Phi}{\delta M}\right)_\Theta=0$ yield

$$\beta M\sin\Theta\cos\Theta = H\sin(\Theta-\Psi), \quad (3a)$$

$$\frac{M-M_0}{\chi_0} + \beta M\cos^2\Theta - H\cos(\Theta-\Psi) = 0. \quad (3b)$$

To analyze the induced magnetization $\Delta M=M(H)-M_0$, we reduce the above equations to a single one

$$\Delta M = \chi_0[H\cos(\Theta-\Psi) - H_a\cos^2\Theta]. \quad (4)$$

The two terms in square brackets account for the effects of the external and anisotropy field, correspondingly. The analytical solution of Eq. (3) is cumbersome; hence, we consider

 

simplifications which occur in extreme cases.

(i) Parallel orientation, $\Psi = \pi/2$:

$$\Theta = \pi/2, \quad \chi = \chi_0, \quad \Delta M_{parallel} = \chi_0 H. \tag{5}$$

(ii) Perpendicular orientation, $\Psi = 0$:

(a) Low field, $H < H_a$:

$$\cos\Theta = \frac{H}{H_a}, \quad \chi = 0, \quad \Delta M_{perp}^{low} = 0. \tag{6}$$

Although the magnetization is not orthogonal to the external field, the induced magnetization is zero. Indeed, the induced magnetization is determined by the internal rather than by the external field. In the perpendicular orientation, the internal field in exactly zero for $H < H_a$.

(b) High field, $H > H_a$:

$$\Theta = 0, \quad \chi = \chi_0, \quad \Delta M_{perp}^{high} \approx \chi_0 (H - H_a). \tag{7}$$

(iii) Intermediate angles:

(a) Low field, $H \ll H_a$: Since the magnetization is almost parallel to the film, then

$$\Theta \approx \pi/2, \quad \Delta M = \chi_0 H \sin\Psi. \tag{8}$$

The susceptibility $\chi(H,\Theta) = \frac{\partial M}{\partial H}$ exhibits discontinuity at zero field,

$$\chi_+ - \chi_- = 2\chi_0 |\sin\Psi|. \tag{9}$$

(b) High field, $H \gg H_a$: Since the magnetization is almost collinear with the field, then

$$\Theta \approx \Psi + \frac{H_a \sin\Psi \cos\Psi}{H - H_a \cos 2\Psi}, \tag{10}$$

$$\Delta M \approx \chi_0 H \left(1 - \frac{H_a \cos^2\Psi}{H + H_a \sin^2\Psi}\right), \tag{11}$$

$$\frac{\chi}{\chi_0} = 1 - \left(\frac{H_a \sin\Psi \cos\Psi}{H + H_a \sin^2\Psi}\right)^2. \tag{12}$$

### B. Ferromagnetic film in oblique field: Magnetoconductance

We wish to calculate conductivity of a thin ferromagnetic film in oblique magnetic field having in mind manganite compounds. Magnetic field is responsible for the colossal and anisotropic magnetoconductance.

*Colossal magnetoconductance* in manganites is usually attributed to the double-exchange mechanism. According to this scenario, the conductivity is determined by the magnitude of magnetization and is almost independent of its orientation with respect to crystallographic axes,[1,9–11]—in other words, $\sigma = \sigma(M^2)$.[12,13] We consider the temperatures not too close to $T_C$ and moderate fields $H < 1$ T when the magnetoconductance is small compared to the zero-field conductance.[14–16] Then, the relation between the magnetoconductance, $\Delta\sigma(H) = \sigma(H) - \sigma_0$, and magnetoresistance, $\Delta\rho(H) = \rho(H) - \rho_0$, is especially simple: $\frac{\Delta\rho(H)}{\rho_0} = -\frac{\Delta\sigma(H)}{\sigma_0}$, where $\rho_0$ and $\sigma_0$ are zero-field resistivity and conductivity. From

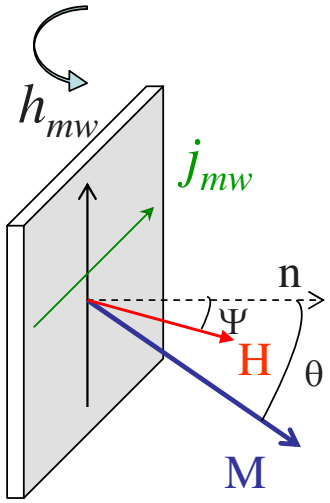


FIG. 1. (Color online) Experimental setup. The sample, which is a thin film on substrate, is firmly attached to the sample holder and is mounted in the center of the resonant cavity, in the antinode of microwave magnetic field. The dc magnetic field $H$ is perpendicular to the microwave magnetic field $h_{mw}$ and is oriented at an angle $\Psi$ with respect to the film normal. This angle can be varied by rotating the sample.

now on we focus on the magnetoconductance and write

$$\sigma(H) \approx \sigma_0 + \left(\frac{d\sigma}{dM}\right)_{H=0} \Delta M(H). \tag{13}$$

We substitute Eq. (4) into Eq. (13) and find

$$\Delta\sigma^{CMR} = \sigma(H) - \sigma_0 \approx \chi_0 \frac{d\sigma}{dM}[H\cos(\Theta - \Psi) - H_a \cos^2\Theta]. \tag{14}$$

Equation (14) depicts a positive magnetoconductance whose magnitude is determined by the factor $\chi_0 \frac{d\sigma}{dM}$ (here, $\chi_0$ is the ionic part of the magnetic susceptibility in the ferromagnetic state that arises from incomplete spin polarization of Mn ions at finite temperature and does not include the Pauli susceptibility of charge carriers) and whose field and angular dependences are determined by the terms in square brackets. Equation (14) improves the previous result of O'Donnell *et al.*[17] who did not consider the term $H_a \cos^2\Theta$ arising from the demagnetizing and anisotropy fields.

*Anisotropic magnetoconductance* can be written as follows:[17]

$$\sigma^{AMR} = (1 - b\sin^2\Theta_J)\sigma_0, \tag{15}$$

where $\sigma_0$ is the (field-dependent) conductivity when the current is parallel to magnetization, $\Theta_J$ is the angle between the magnetization and the current, and $b$ is a small dimensionless constant which has positive sign in manganites.[9,10] In the common magnetic resonance geometry the microwave current is predominantly oriented perpendicularly to the rotation axis (Fig. 1). Then for negligible in-plane anisotropy and for oblique field orientation we find $\Theta_J \approx 90° - \Theta$. The conductivity in magnetic field is

$$\sigma(H) = (1 - b\cos^2\Theta)\sigma_0. \tag{16}$$

The field dependence of the conductivity arises from the term $\sigma_0(H)$—this is due to colossal magnetoresistance; and since the angle $\Theta$ can be field dependent, from the term $b\cos^2\Theta$ that accounts for the anisotropic magnetoresistance. The CMR is a strong effect which appears at all field orientations and results in conductivity linearly increasing with field that comes to saturation at high field on the order of a few tesla. On the other hand, the anisotropic magnetoresistance (AMR) is a weak effect which is prominent only at oblique field orientation and it comes to saturation in a relatively small field, $H \sim H_a$ (less than 0.5 T). Hence, at high field the CMR makes the dominant contribution, while at low-field and oblique-field orientation the CMR and AMR contributions may be comparable.

### C. Nonresonant microwave absorption and magnetoresistance

The inductive methods for measuring magnetoresistance are advantageous since they are contactless and allow for the sample rotation in magnetic field. This is most easily realized using a cavity perturbation technique where conducting sample is mounted off center in the resonant cavity[2] or in the antinode of the microwave electric field.[3,18,19] We consider here a different setup where the sample is mounted in the antinode of the microwave magnetic field. Although this corresponds to the electric field node, Zhai *et al.*[20] showed that the conductivity may be measured in this configuration as well. We prefer this setup since it allows for the measurement of the resonant magnetic susceptibility as well.

For the qualitative analysis of our measurements we follow Ref. 21 and consider the complex magnetic susceptibility of an infinite conducting film in a uniform parallel microwave field,

$$\chi_{mw} = (1 + \chi_{int})\frac{(\sinh u + \sin u) + i(\sinh u - \sin u)}{u(\cosh u + \cos u)} - 1. \tag{17}$$

Here, $\chi_{int}$ is the intrinsic microwave magnetic susceptibility of the film, $d$ is the film thickness, $\delta = (2/\mu\omega\sigma)^{1/2}$ is the skin depth, $\omega$ is the microwave frequency, $\mu = \mu_0(1+\chi_{int})$ is the intrinsic magnetic permeability, and $u = d/\delta$. For a thin film, $u \ll 1$, Eq. (17) reduces to

$$\chi_{mw} \approx \chi_{int} - \frac{u^4}{30} + i\frac{u^2}{6}. \tag{18}$$

The first term in Eq. (18) corresponds to intrinsic microwave susceptibility. It is non-negligible only at the field corresponding to the ferromagnetic resonance. The resonance field is found from the well-known expression[22]

$$\left(\frac{\omega}{\gamma}\right)^2 = [H_{res}\cos(\Theta - \Psi) - H_a\cos^2\Theta] \times [H_{res}\cos(\Theta - \Psi) - H_a\cos 2\Theta]. \tag{19}$$

The second and third terms in Eq. (18) account for the eddy-current contribution to the real and imaginary parts of magnetic susceptibility, correspondingly (see also Ref. 23). To estimate this nonresonant contribution we neglect $\chi_{int}$ in Eq. (18) and find

$$\chi''_{mw} \approx \frac{\mu_0\omega\sigma d^2}{12}, \tag{20a}$$

$$\chi'_{mw} \approx \frac{\mu_0^2\omega^2\sigma^2 d^4}{120} \ll \chi''_{mw}. \tag{20b}$$

Equation (20b) indicates that the eddy-current contribution to the real part of the thin-film susceptibility is negligible, while Eq. (20a) shows that the lossy part of the effective magnetic susceptibility of a thin film is proportional to the conductivity (this is in contrast to thick films where it is proportional to the resistivity[20]). Therefore, by measuring the $\chi''_{mw}$ of a thin film one can find its conductivity.

## III. EXPERIMENT

### A. Samples

We studied thin epitaxial $La_{0.7}Sr_{0.3}MnO_3$ films ($d$=50, 100, 150, and 200 nm) on a (001) $SrTiO_3$ substrate and $La_{0.67}Sr_{0.33}MnO_3$ films ($d$=50 and 150 nm) on a $NdGaO_3$ substrate. The films were grown by the pulsed laser deposition technique in two different laboratories[24,25] and cut to small $1\times1$ mm$^2$ pieces in order to keep a reasonable value of the cavity $Q$–factor. The film thickness is much smaller than the skin depth at 10 GHz ($\delta$=22 $\mu$m at 295 K and $\delta$=5 $\mu$m at 50 K). Although the $T_C$ and coercive field of the samples were different, almost all of them showed measurable microwave magnetoconductance. Most of the results shown here were obtained using 200-nm-thick $La_{0.7}Sr_{0.3}MnO_3$ films on $SrTiO_3$.

### B. Basics of the ESR spectrometer

We utilized a bipolar Bruker ESR spectrometer operating at 9.4 GHz, a $TE_{102}$ resonant cavity, and an Oxford cryostat. The sample is mounted in the cavity center. The microwave bridge measures reflected signal from the cavity with the sample. The bridge is balanced and the cavity is critically coupled at $H$=0. The dc magnetic field is then slowly swept. If the complex microwave magnetic susceptibility of the sample, $\chi_{mw}$, depends on magnetic field, the condition of critical coupling is violated and a reflected signal appears:

$$P \propto \chi_{mw}(H)\,\eta Q. \tag{21}$$

Here $Q$ is the $Q$ factor of the cavity, $\eta \approx V/V_c$ is the filling factor, $V$ is the sample volume, and $V_c$ is the cavity volume. The phase setting of the microwave detector chooses either absorption, $P_{abs} \propto \chi''_{mw}$, or dispersion, $P_{disp} \propto \chi'_{mw}$. To achieve high sensitivity, the dc field is modulated and the modulated reflection

$$S_{mod} = \frac{dP}{dH}H_{mod} \tag{22}$$

is measured using a lock-in detector. Here, $H_{mod}$ is the amplitude of the modulation field. To find the absolute reflectivity, the modulated reflection is integrated,

$$P(H) = P(H_0) + \frac{1}{H_{mod}} \int_{H_0}^{H} S_{mod} dH. \quad (23)$$

Here $H_0$ is the lower limit of the dc field sweep and $P(H_0)$ should be determined independently.

### C. Extraction of the genuine signal

In the context of ESR spectroscopy, the nonresonant microwave absorption is represented by the modulation signal base line that consists of several contributions:

$$S_{mod} = S_{bridge} + S_{vibr} + S_{sample}. \quad (24)$$

(i) $S_{bridge}$, a constant offset that originates from the electronics of the microwave bridge. We use a symmetric (with respect to the zero) field sweep, find the average signal $S_{ave}$, and subtract it from our results. Since $S_{vibr}$ and $S_{sample}$ are odd functions of the field, they do not contribute to the average signal; hence, $S_{bridge}=S_{ave}$.

(ii) $S_{vibr} \propto I_{mod} H$. This contribution comes from the cavity wall vibration. Indeed, when the ac current $I_{mod}$ flows through the modulation coils (they are usually firmly attached to cavity walls) the cavity acquires periodic deformation in the dc magnetic field $H$. The shape of the cavity and its resonant frequency are modulated, the condition of critical coupling is periodically violated, and there appears a reflected signal that is proportional to the mechanical force on cavity walls. This parasitic contribution linearly depends on field and can be easily taken for the magnetoresistance signal.

To eliminate the vibration contribution $S_{vibr}$, we choose a special phase setting of the lock-in detector. Indeed, since the vibration signal is phase shifted with respect to the modulation current (most probably due to proximity of the modulation frequency to mechanical resonances of the cavity), it is maximized at a certain phase setting of the lock-in detector, $\psi \neq 0$. However, the genuine signal, arising from magnetoconductance in the sample, is in phase with the modulation field and it is maximized when $\psi=0$. Therefore, by setting the lock-in detector phase in quadrature with the vibration signal we eliminate the latter. Although the magnitude of the genuine signal is also diminished by $\cos \psi$, it does not disappear completely.

To verify the elimination of the vibration contribution we analyze the dispersion signal. Note that vibration contributions into absorption and dispersion signals are comparable, while magnetoconductance contributes mostly to the absorption signal [Eq. (20)]. Therefore, the test for the proper choice of the lock-in detector phase is that the linear base lines in derivative dispersion and absorption signals disappear simultaneously.

(iii) $S_{sample}$ is the genuine signal which arises from the microwave absorption in the sample. The nonresonant absorption signal associated with the conductor loss is found from Eqs. (20a), (21), and (22):

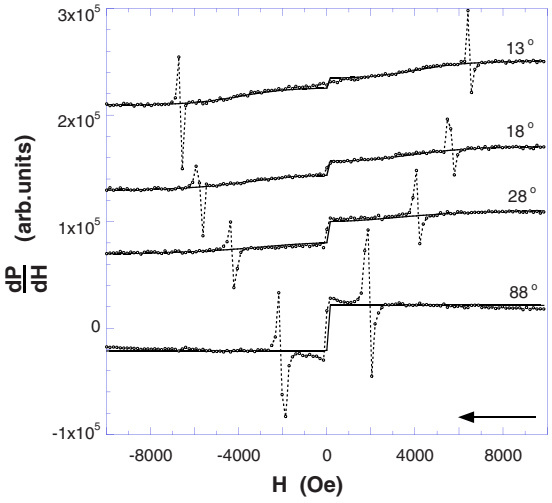


FIG. 2. (Color online) Absorption derivative at different orientations of the magnetic field. $\Psi=0°$ and $\Psi=90°$ stand for the perpendicular and parallel orientations, correspondingly. The arrow shows the direction of the field sweep. Modulation field is 10 Oe. The experimental data are shown by small circles. The sharp peaks correspond to the ferromagnetic resonance, while the broad antisymmetric base line originates from the microwave magnetoconductance. The solid lines show the model prediction for the base line. Two fitting parameters have been used for all curves: anisotropy field $H_a=3900$ Oe and high-field absorption derivative in the parallel geometry, $\frac{dP}{dH}=2.1\times10^4$.

$$S_{sample} = \frac{d\sigma}{dH} \frac{\mu_0 \omega d^2 \eta Q H_{mod}}{12}. \quad (25)$$

It consists of the field derivative of the conductivity, $\frac{d\sigma}{dH}$, multiplied by a constant factor. To find conductivity we integrate Eq. (25). The results are analyzed using Eqs. (3) and (4).

## IV. EXPERIMENTAL RESULTS AND COMPARISON TO THE MODEL

### A. Derivative microwave absorption

Figure 2 shows derivative microwave absorption at several field orientations for a $La_{0.7}Sr_{0.3}MnO_3$ film on the $SrTiO_3$ substrate.[24] We observe a sharp ferromagnetic resonance (FMR) signal superimposed on a wide antisymmetric base line. For the parallel-field orientation the base line may be represented as a step function which reverses its sign at zero field. For the oblique-field orientation, the base line varies with field more gradually and the zero-field discontinuity becomes smaller. When the field deviation from the perpendicular orientation is less than 10°, there appears pronounced zero-field absorption associated with magnetic domains. It will be discussed elsewhere.[26] In this study we focus on the base line which we attribute to microwave magnetoconductance.

The model prediction based on Eqs. (3a), (3b), and (14) fits the base line fairly well (see solid lines in the Fig. 2). For the whole family of $\frac{dP(H,\Theta)}{dH}$ dependences there are only two

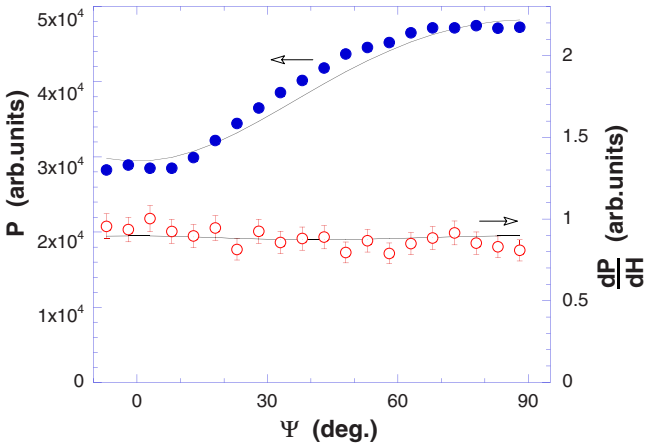


FIG. 3. (Color online) Angular dependence of the integrated absorption (solid symbols) and absorption derivative (open symbols) at $H=1$ T as inferred from Figs. 2 and 4. The solid lines show model prediction based on Eqs. (11) and (12) and $H_a=3900$ Oe.

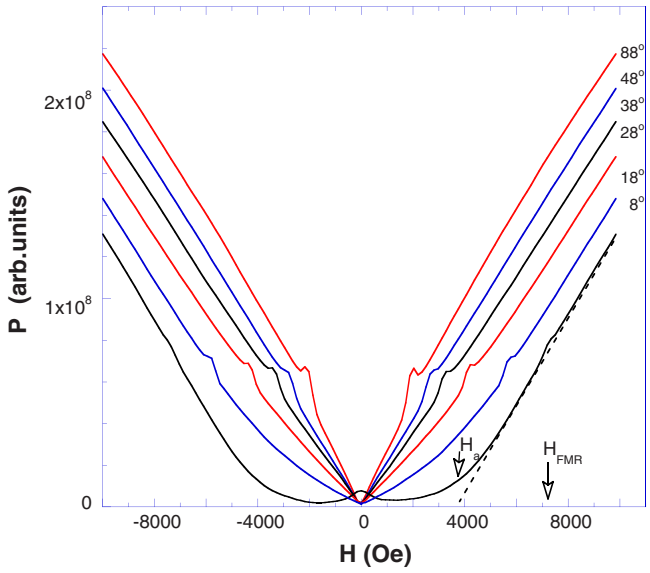


FIG. 4. (Color online) Integrated absorption at different orientations of the magnetic field as found from the integration of the data of the Fig. 2. The curves for different orientations are vertically shifted to achieve the same value of minimal absorption. The numbers at each curve show the polar angle of the field, whereas $\Psi=0°$ and $\Psi=90°$ stand for the perpendicular and parallel orientations, correspondingly. The dashed line shows linear approximation for the high-field data for (almost) perpendicular orientation. The horizontal intercept yields the anisotropy field $H_a$.

fitting parameters: the high-field absorption derivative in the parallel orientation and the effective anisotropy field $H_a^{MR}=3900$ Oe. The latter is somewhat lower than the anisotropy field $H_a^{FMR}=4300$ Oe found from the ferromagnetic resonance using Eq. (19) and Fig. 2. The difference may arise from the variation of the anisotropy field across the film.

Figure 3 shows the angular dependence of the derivative microwave absorption at high field $H=1$ T. This very weak dependence is consistent with the model prediction [Eq. (12)].

### B. Integrated microwave absorption

To compare integrated absorption at different orientations we integrated the data of the Fig. 2 using Eq. (23). The main difficulty here is to find $P(H_0)$ [Eq. (23)] which can depend on orientation. We performed integration with arbitrary reference field and plotted the resulting curves for all orientations at the same plot. Different choices of $P(H_0)$ correspond to vertical shifts of the curves [Eq. (23)]. We shift each curve vertically to achieve the same value of the minimal absorption. Figure 4 shows our results. We observe (i) superlinear field dependences which we attribute to magnetoconductance and (ii) a small high-field bump arising from the ferromagnetic resonance. The superposition of both kinds of absorption in the same experimental run unambiguously proves the positive sign of magnetoconductance in LSMO. Figure 3 shows the angular dependence of the integrated absorption at high field. The experimental data agree well with the model prediction [Eqs. (11)], and this is an additional proof that the nonresonant microwave absorption arises from magnetoconductance.

We consider now the curve for the almost perpendicular orientation $\Psi=8°$ (Fig. 4). When $H<4000$ Oe, the CMR contribution is negligible since the internal field is zero [Eq. (6)]. However, there is some low-field absorption which corresponds to negative magnetoconductance. A similar feature was observed in dc-transport measurements in $La_{0.7}Ca_{0.3}MnO_3$ films[27] and was attributed to anisotropic magnetoresistance. The AMR can explain our results as well, although ferromagnetic resonance in the multidomain state[28] seems to be a more plausible explanation here.

### C. Dispersion

Figure 5 compares integrated absorption and dispersion for nearly parallel orientation. With respect to the ferromagnetic resonance contribution, it is clearly seen that the magnitude of the absorption peak at $H_{FMR}=2000$ Oe is equal to the peak-to-peak magnitude of the dispersion peak, as expected for the Lorentzian resonance.

With respect to the nonresonant eddy-current contribution, it appears only in the absorption signal and is absent in the dispersion signal. This conclusion is further verified by the inspection of the low-field derivative signals which are measured with higher sensitivity. Figure 6 shows that absorption derivative exhibits a sharp zero-field discontinuity [this is a signature of magnetoresistance—see Eq. (9)] while the dispersion derivative varies smoothly across zero, showing no trace of the magnetoresistance contribution. This is consistent with Eq. (20), which for our films yields $\chi'/\chi''=d^2/5\delta^2\sim 10^{-4}$.

### D. Temperature dependence

To characterize microwave magnetoconductance at different temperatures we chose the factor $\frac{\partial P}{\partial H}$. Equations (14) and (25) yield that in the parallel geometry this factor is field

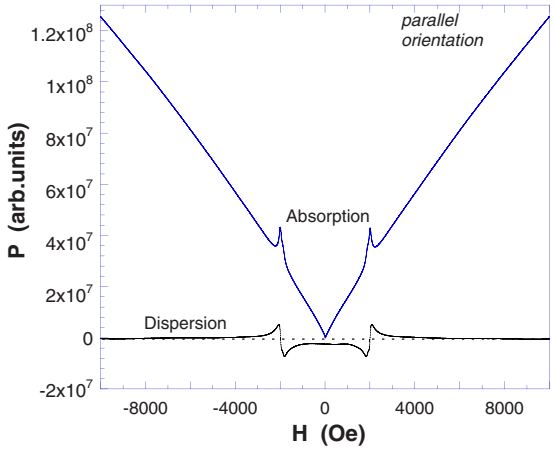


FIG. 5. (Color online) Integrated absorption and dispersion in the parallel geometry for a 200-nm-thick $La_{0.7}Sr_{0.3}MnO_3$ film on $SrTiO_3$ (Ref. 24). Absorption signal exhibits ferromagnetic resonance at 2000 Oe superimposed on the broad base line that linearly depends on field. Dispersion signal exhibits only ferromagnetic resonance and does not show any baseline.

independent and $\frac{\partial P}{\partial H} \propto \frac{\partial \sigma}{\partial M}$; hence, it is a direct measure of the magnetoconductance. Figure 7 shows temperature dependence of $\frac{dP}{dH}$ as well as that of the anisotropy field. The latter was found from the ferromagnetic resonance data in the same sample. It should be noted that for our thin films the anisotropy field is dominated by the shape anisotropy and, therefore, it can serve as a direct measure of magnetization.

Figure 7 shows that magnetoconductance exhibits a sharp peak around 300 K and becomes very small at low temperatures. This temperature dependence is very similar to that for CMR found in transport measurements on high-quality epitaxial $La_{0.7}Sr_{0.3}MnO_3$ films[14–16] and indicates an intrinsic

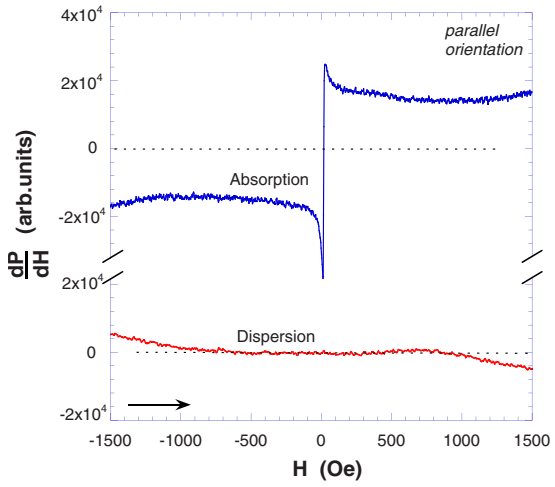


FIG. 6. (Color online) Absorption derivative and dispersion derivative in the parallel geometry. Note the zero-field discontinuity in absorption as opposed to the smooth variation of dispersion. The black arrow shows direction of the field sweep. Modulation field $H_{mod}$=10 Oe is high to achieve enough sensitivity for dispersion measurement. This leads to some distortion in the absorption curve due to overmodulation.

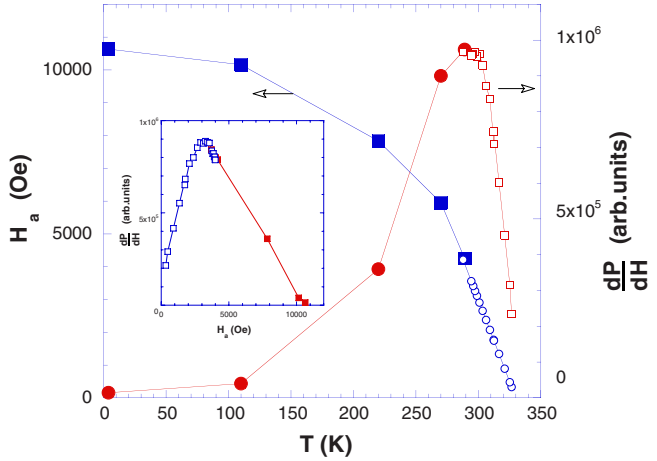


FIG. 7. (Color online) Temperature dependence of the effective anisotropy field $H_a$ and of the magnetoconductance $\frac{dP}{dH}$ at $H$=1 T. The inset shows dependence of the derivative absorption on the anisotropy field. Solid symbols stand for the sample LSMO55-1-A. Here, the measurements were performed at several fixed temperatures and at low microwave power of −30 dB. Open symbols stand for the sample LSMO55-1-B (both samples were cut from the same film). Here, the measurements were performed at ambient temperature and at different microwave power levels from −30 dB to 0 dB. In this case the temperature of the sample increases due to self-heating. It was estimated indirectly from the position of the FMR peak.

mechanism. The inset to Fig. 7 shows how magnetoconductance depends on the anisotropy field (in other words, on magnetization).

It should be noted that the low-temperature measurements were performed with one sample while the measurements above room temperature were performed with another sample which was cut from the same film. While the low-temperature measurements were performed at several fixed temperatures and low microwave power to exclude self-heating, the measurements above 295 K were performed at ambient temperature and increased microwave power. In this case the sample temperature is enhanced due to self-heating. In these latter measurements we directly measure the magnetoconductance and the anisotropy field while the sample temperature was estimated using the data from the inset to the Fig. 7 assuming a linear temperature dependence of the anisotropy field in the vicinity of $T_C$.

### E. Low-field range

Figure 8 shows low-field integrated absorption and absorption derivative in the parallel orientation. There is a pronounced hysteresis. The absorption derivative exhibits a discontinuity that corresponds to the cusp in the integrated absorption. When the field orientation deviates from the parallel orientation, the magnitude of the discontinuity becomes smaller (Fig. 2) and its position moves to higher field (Fig. 9). To account for the angular dependence of the discontinuity we note that in low field $H \ll H_a$, where magnetization is nearly parallel to the film, the discontinuity should occur

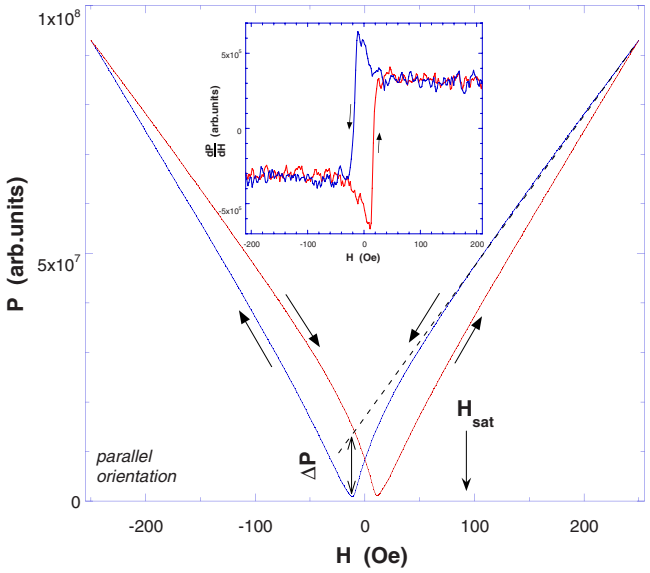


FIG. 8. (Color online) Low-field absorption: integrated (main panel) and derivative (inset). The direction of field sweep is shown by arrows. The derivative absorption exhibits low-field discontinuity that is preceded by a sharp dip or peak. The integrated absorption exhibits the cusp and the drop $\Delta P$, correspondingly. The dashed line shows linear extrapolation of the high-field data to the low-field region. Deviation of the data from the linear dependence indicates the in-plane saturation field $H_{sat}$. The width of the hysteresis loop yields coercive field $H_c=11$ Oe. We used here a very slow sweep rate and small modulation field $H_{mod}=0.5$ Oe to prevent overmodulation.

when the parallel component of the field is equal to coercive field, $H_{\|}=H\sin\Psi=H_c$. Indeed, the angular dependence $H_{disc}=\frac{H_c}{\sin\Psi}$ describes our data perfectly well (the solid line in Fig. 9). We find $H_c=11$ Oe, and this is in good agreement with superconducting quantum interference device (SQUID) measurements on the same film. The $H_c$ found in our measurements increases at low temperatures ($H_c=23$ Oe at 219 K and $H_c=50$ Oe at 4.2 K), which is consistent with magnetization measurements for similar films.[29]

The deviation of the low-field integrated absorption from the linear dependence predicted by Eq. (5) (see low-field region in Fig. 8) corresponds to a conductance drop. Similar low-field features in the magnetically unsaturated state were observed in microwave studies of thin Fe-Cr films[31–33] and in dc-transport measurements in $La_{0.7}Ca_{0.3}MnO_3$ (Refs. 17 and 37) and $La_{0.85}Sr_{0.15}MnO_3$ thin films.[35] The low-field conductance drop in the magnetically unsaturated state can be related to the (i) domain wall resistance,[30] (ii) ferromagnetic resonance in the multidomain state,[28] or (iii) anisotropic magnetoresistance.[17,34,35] We attribute the low-field absorption in the nearly perpendicular orientation $\Psi<10°$ to the ferromagnetic resonance in the multidomain state,[26] while the conductance drop observed at $\Psi>10°$ (Fig. 8) is attributed to anisotropic magnetoresistance.

Indeed, at high field the film is in the single-domain state and the projection of magnetization on the film plane is parallel to the microwave current (Fig. 1); hence, $\Theta_J=0$ and Eq. (15) yields $\sigma=\sigma_0$. However, when the in-plane field is below the in-plane saturation field, $H<H_{sat}$, the magnetization aligns along the easy in-plane axes and is not parallel to the current anymore. Equation (15) yields $\sigma=(1-b\sin^2\Theta_J)\sigma_0$. Therefore, when the field becomes smaller than the in-plane saturation field, there is a conductance drop $\Delta\sigma\sim-b\sigma_0$, which does not depend on the polar angle of the field, $\Psi$. This is in agreement with our observations (Figs. 8 and 9). Following this interpretation, the onset for the deviation from the linear dependence predicted by Eq. (14) indicates the saturation field. Figure 8 yields $H_{sat}=90-100$ Oe, in good agreement with $H_{sat}=90$ Oe found in magnetization measurements on similar films.[36]

### F. Comparison between the samples

Almost all our films demonstrated measurable magnetoconductance. The field and angular dependences for the films fabricated in different laboratories were much more the same. Indeed, Figs. 5 and 10 show the microwave magnetoconductance for two epitaxial $La_{0.7}Sr_{0.3}MnO_3$ films on the $SrTiO_3$, which were fabricated in different laboratories. The field dependence of the nonresonant microwave absorption is very similar, although the resonant absorption is different.

## V. DISCUSSION

We verified our model and demonstrated that magnetoresistance is determined by the dc magnetic susceptibility in the ferromagnetic state. This offers the possibility of measuring the magnetostatic properties of magnetic films using contactless microwave methods, as was suggested earlier in Ref. 37. In such a way we were able to measure coercive field (Fig. 9), the in-plane saturation field, and the in-plane aniso-

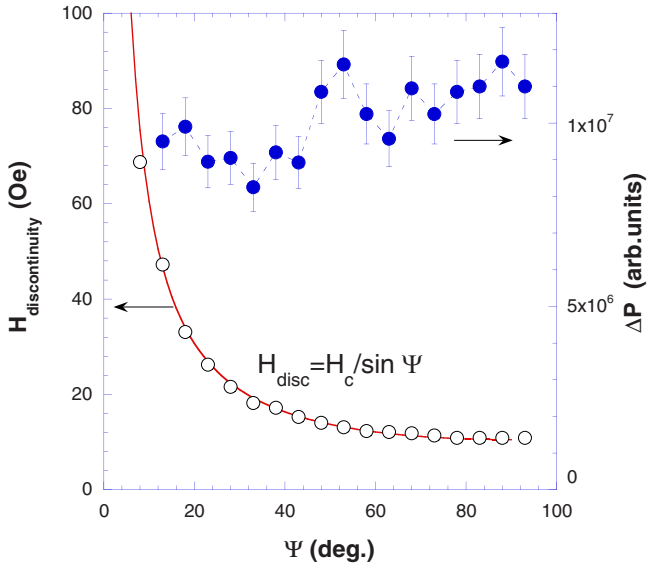


FIG. 9. (Color online) Angular dependence of the discontinuity field and of the low-field absorption drop $\Delta P$ (from the data of Fig. 8). The solid line shows model prediction while the dashed line is the guide to the eye. The $H_{disc}$ is strongly angular dependent while the $\Delta P$ is not. We attribute $H_{disc}$ to the coercive field and $\Delta P$ to the anisotropic magnetoresistance in the magnetically unsaturated state.

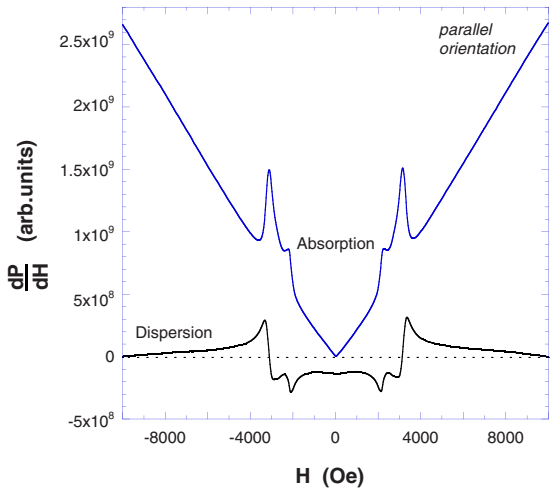


FIG. 10. (Color online) Integrated absorption and dispersion in the parallel geometry for a 100-nm-thick $La_{0.7}Sr_{0.3}MnO_3$ film on $SrTiO_3$ (Ref. 25). Note similarity to Fig. 5. The film is slightly nonuniform and the FMR peak is split in two.

tropy field (not shown here). In what follows we estimate the out-of-plane anisotropy field from the nonresonant microwave absorption. Indeed, for the integrated microwave absorption in the perpendicular orientation, Eq. (7) yields a superlinear field dependence with the horizontal intercept equal to the anisotropy field. We extrapolate our data (Fig. 4) to low field and find $H_a^{MR}=3900$ Oe. This is reasonably compared to the anisotropy field found from the ferromagnetic resonance as given by Eq. (19)—namely, $H_a^{FMR}=4300$ Oe.

In what follows we apply our approach to the data of Liu and Furdyna[38] who measured the ferromagnetic resonance in magnetic semiconductors. The inset in Fig. 11 shows the absorption derivative in the perpendicular geometry for a thin GaMnAs film.[38] There is a ferromagnetic resonance accompanied with several spin-wave resonances and a broad base line that Ref. 38 attributed to magnetoresistance. We integrate these data assuming that the absorption derivative for $H<2$ kOe is negligibly small. Figure 11 shows the field dependence of the integrated absorption found in such a way. It is very similar to what is shown in Fig. 4 for a manganite film. We approximate the high-field data of the Fig. 11 by a linear dependence. The horizontal intercept yields $H_a^{MR}=3700$ Oe while the FMR yields somewhat higher value, $H_a^{FMR}=4300$ Oe. The difference may arise from slight deviation from the perpendicular orientation, mosaicity, the spread of the magnitude of the anisotropy field across the film, and some ambiguity in the determination of the magnitude of the zero-field absorption.

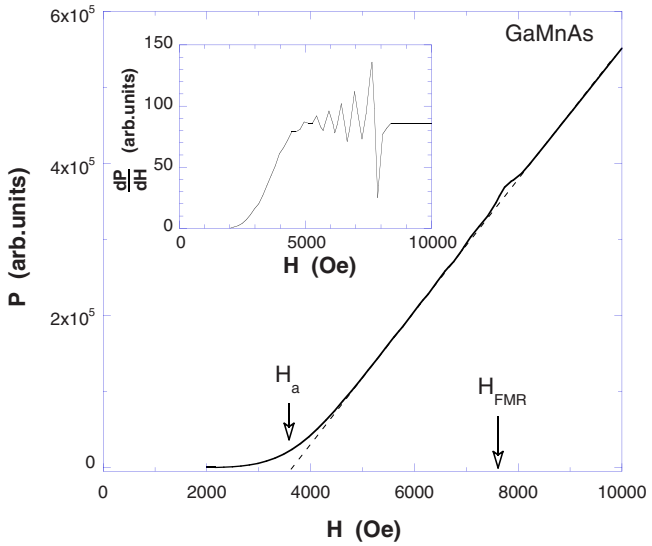


FIG. 11. (Color online) The inset shows derivative microwave absorption in the perpendicular geometry for a 200-nm-thick $Ga_{0.924}Mn_{0.076}As$ film (replotted using the data of Ref. 38). The main panel shows integrated absorption calculated using the data of the inset and assuming that the absorption derivative at $H<2$ kOe is negligibly small. The dashed line shows the linear approximation for high field. The intercept of this line with the horizontal axis yields the anisotropy field $H_a=3700$ Oe.

## VI. CONCLUSIONS

We demonstrate how to measure magnetoresistance in a contactless way using a bipolar ESR spectrometer. We develop a model accounting for the magnetoresistance of a thin ferromagnetic film in oblique magnetic field. Our model is in excellent agreement with our measurements. We show that the intrinsic magnetoresistance in $La_{0.7}Sr_{0.3}MnO_3$ films is determined by the magnitude of magnetization and is insensitive to its orientation with respect to the film and to the crystallographic axes. Our approach to measure magnetoresistance using a microwave technique can be useful for other conducting magnetic materials.

## ACKNOWLEDGMENTS

We are grateful to Denis Golosov and Lior Klein for helpful discussions and to Xiangzhen Xu for help with the handling of the samples.

*Permanent address: the Racah Institute of Physics, the Hebrew University of Jerusalem, 91904 Jerusalem, Israel.

†Permanent address: University of Cassino, Dipartimento di Meccanica Strutture Ambiente e Territorio, Facolta'di Ingegneria, via G. Di Biasio, 43, 03043 CASSINO (FR), Italy.

[1] M. B. Salamon and M. Jaime, Rev. Mod. Phys. **73**, 583 (2001).

[2] S. D. Tyagi, S. E. Lofland, M. Dominguez, S. M. Bhagat, C. Kwon, M. C. Robson, R. Ramesh, and T. Venkatesan, Appl. Phys. Lett. **68**, 2893 (1996).

[3] M. C. Robson, C. Kwon, S. E. Lofland, S. B. Ogale, S. M.

Bhagat, M. Rajeswari, T. Venkatesan, R. Ramesh, J. Electroceram. **4**, 167 (2000).
[4] F. J. Owens, Physica C **353**, 265 (2001).
[5] S. E. Lofland, S. M. Bhagat, H. L. Ju, G. C. Xiong, T. Venkatesan, and R. L. Greene, Phys. Rev. B **52**, 15058 (1995).
[6] S. Budak, M. Ozdemir, B. Aktas, Physica B **339**, 45 (2003).
[7] D. L. Lyfar, S. M. Ryabchenko, V. N. Krivoruchko, S. I. Khartsev, and A. M. Grishin, Phys. Rev. B **69**, 100409(R) (2004).
[8] H. Enriquez, N. Bontemps, P. Fournier, A. Kapitulnik, A. Maignan, and A. Ruyter, Phys. Rev. B **53**, R14757 (1996).
[9] M. Ziese, Rep. Prog. Phys. **65**, 143 (2002).
[10] E. Favre-Nicolin and L. Ranno, J. Magn. Magn. Mater. **272**, 1814 (2004).
[11] H. S. Wang, Qi Li, Kai Liu, and C. L. Chien, Appl. Phys. Lett. **74**, 2212 (1999).
[12] M. F. Hundley, M. Hawley, R. H. Heffner, Q. X. Jia, J. J. Neumeier, J. Tesmer, and J. D. Thompson, X. D. Wu, Appl. Phys. Lett. **67**, 860 (1995).
[13] Y. Tokura and Y. Tomioka, J. Magn. Magn. Mater. **200**, 1 (1999).
[14] X. W. Li, A. Gupta, Gang Xiao, and G. Q. Gong, Appl. Phys. Lett. **71**, 1124 (1997).
[15] R. Mathieu, P. Svedlindh, R. A. Chakalov, and Z. G. Ivanov, Phys. Rev. B **62**, 3333 (2000).
[16] L. Reversat, P. Crozat, R. Lyonnet, C. Dupas, and J. P. Contour, Appl. Phys. Lett. **83**, 2596 (2003).
[17] J. O'Donnell, M. Onellion, M. S. Rzchowski, J. N. Eckstein, and I. Bozovic, Phys. Rev. B **55**, 5873 (1997).
[18] V. V. Srinivasu, S. E. Lofland, S. M. Bhagat, K. Ghosh, and S. D. Tyagi, J. Appl. Phys. **86**, 1067 (1999).
[19] S. Sarangi and S. V. Bhat, Rev. Sci. Instrum. **78**, 023905 (2005).
[20] Z. Zhai, C. Kusko, N. Hakim, S. Sridhar, A. Revcolevschi, and A. Vietkine, Rev. Sci. Instrum. **71**, 3151 (2000).
[21] V. B. Geshkenbein, V. M. Vinokur, and R. Fehrenbacher, Phys. Rev. B **43**, 3748 (1991).
[22] A. G. Gurevich and G. A. Melkov, *Magnetization Oscillations and Waves* (CRC Press, Boca Raton, 1996), p. 19.
[23] The resonant susceptibility is also affected by the finite conductivity. This leads to a Dysonian line shape arising from the mixing of the dispersive and absorptive parts of the resonant susceptibility.
[24] K. Senapati and R. C. Budhani, Phys. Rev. B **71**, 224507 (2005).
[25] F. Yang, L. Mechin, J. M. Routoure, B. Guillet, and R. A. Chakalov, J. Appl. Phys. **99**, 024903 (2006).
[26] M. Golosovsky, P. Monod, and R. C. Budhani (unpublished).
[27] J. N. Eckstein, I. Bozovic, J. ODonnell, M. Onellion, and M. S. Rzchowski, Appl. Phys. Lett. **69**, 1312 (1996).
[28] N. Vucadinovic, J. Ben Youssef, and H. Le Gall, J. Magn. Magn. Mater. **150**, 213 (1995).
[29] P. Lecoeur, Pl. Touilloud, Gang Xiao, A. Gupta, G. Q. Gong, and X. W. Li, J. Appl. Phys. **82**, 3934 (1997).
[30] D. I. Golosov, Phys. Rev. B **67**, 064404 (2003).
[31] Z. Frait, P. Sturc, K. Temst, Y. Bruyneseraede, and I. Vavra, Solid State Commun. **112**, 569 (1999).
[32] J. J. Krebs, P. Lubitz, A. Chaiken, and G. A. Printz, J. Appl. Phys. **69**, 4795 (1991).
[33] J. Dubowick, F. Stobiecki, and I. Goscianska, Czech. J. Phys. **52**, 227 (2002).
[34] J. O'Donnell, J. N. Eckstein, and M. S. Rzchowski, Appl. Phys. Lett. **76**, 218 (2000).
[35] Y. Bason, L. Klein, J.-B. Yau, X. Hong, J. D. Hoffman, and C. H. Ahn, J. Appl. Phys. **99**, 08R701 (2006).
[36] L. M. Berndt, V. Balbarin, and Y. Suzuki, Appl. Phys. Lett. **77**, 2903 (2000).
[37] E. Dan Dahlberg, K. Riggs, and G. A. Prinz, J. Appl. Phys. **63**, 4270 (1988).
[38] X. Liu and J. K. Furdyna, J. Phys.: Condens. Matter **18**, R245 (2006).